# Propagation and Characterization of Novel Graded and Linearly Chirped Type's of Refractive Index Profile Symmetric Planar Slab Waveguide by Numerical Means

**Sanjeev Kumar Raghuwanshi*** and **B. M. Azizur Rahman**

**Abstract**—We characterize the alpha power and chirped types of refractive index profile planar slab waveguide in terms of TE/TM mode study, waveguide dispersion study, mode profile properties, power confinement factor and universal $b$-$V$ graph. Our own developed finite element method has been efficiently applied to analyze the symmetric planar slab waveguide having a complicated refractive index profile. There is a requirement for a high accuracy of numerical technique to analyze the arbitrary refractive index waveguide, as at some frequency the TE and TM modes are smeared on each other, and it is difficult to distinguish them while analyzing. This paper successfully demonstrates the different TE/TM modes supported by the waveguide with respect to alpha-power and linearly chirped types of refractive index profile. The main contribution of our work is to identify the TE/TM mode numerically for a complex refractive index planar slab waveguide and to characterize them in terms of their performance parameters. Then we apply the mode propagation concept to estimate the propagation phenomena in alpha-power and chirped types of refractive index profile waveguide. All the results presented in this paper are simulated in MATLAB only. Our study reveals that waveguide dispersion and number of allowed guided modes are small while for the case of triangular index profile followed by chirped profile and maximum for step index profile case. Hence triangular and chirped types of refractive index profile waveguide seem to be more efficient for long haul optical communication systems.

## 1. INTRODUCTION

The rapid developments in fields such as fiber optics communication engineering and integrated optical electronics have expanded interest and increased expectations about guided wave optics, in which optical waveguides play a central role. Maxwell's equations are used to calculate the propagation characteristics of optical waveguides. It is, however, rather rare to obtain a precise analytic solution, and therefore, an exact analysis of optical waveguide is generally considered to be difficult. For this reason, various methods of optical waveguide analysis have been developed. These methods may be broadly classified into two categories: analytical approximation solutions [1–5] and numerical solution using computers [6–10]. Since optical waveguide having a complicated profile cannot be solved by analytical method, we choose it to be analyzed by Finite Element Method [11–16]. In the microwave band, electromagnetic fields are generally distributed within a finite area surrounded by conductors, as in waveguides and coaxial lines. On the other hand, it is difficult to construct a waveguide mainly from metal in the visible wave band, since the metal will behave as a substance having a complex permittivity with a large absolute value. For this reason, waveguides are usually constructed by combining appropriate
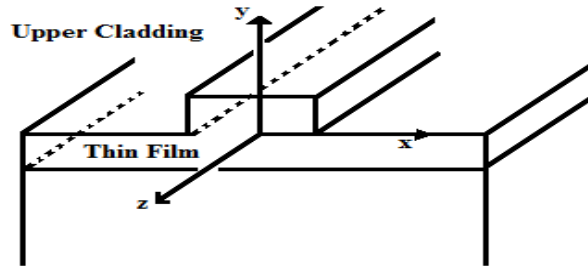
**Figure 1.** Optical waveguide.

dielectrics, as shown in Figure 1, thus distributing an electromagnetic field over an infinite area. By loading a thin film with a higher refractive index than either the substrate or the upper cladding on the substrate surface, the light can be trapped inside this film. Furthermore, as the thickness of the film increases, the effective refractive index sensed by the light increases. Waveguides in which the refractive index changes in stages are called step index (SI) optical waveguides while those with a gradual refractive index change are called graded index (GI) optical waveguides [17–22].

An optical waveguide that is uniform in the direction of propagation, as shown in Figure 1, is the most basic type of waveguide, but this alone is not sufficient for construction of an optical integrated circuit. In reality, arbitrary refractive index profile waveguide can give a better performance in light guiding characteristics. Optical waveguide may be classified roughly into two sharp categories: single mode (SM) optical waveguide which allow only one mode (of a given polarization), and multi-mode (MM) optical waveguide with multi-mode propagation [23–33]. Optical waveguide having an arbitrary refractive index profile can have an excellent connecting and bending characteristics as well as dispersion control performance. This paper addresses these issues with proper simulation results in MATLAB platform. Here we have avoided the problem formulation part by using finite element method, as it is widely discussed in our recently published papers [7, 27].

## 2. ANALYSIS OF GRADED REFRACTIVE INDEX PROFILE PLANAR SLAB WAVEGUIDES

When eigen-value $\beta$ of a tri-diagonal matrix is obtained, the corresponding eigenvector $R_0$, $R_1$, ..., $R_N$ is calculated by the matrix operation. Here $R_0$ can be determined when we normalize the total optical power $P$ carried by the mode to 1. Figure 2 shows the schematic of the $\alpha$-power refractive-index profiles
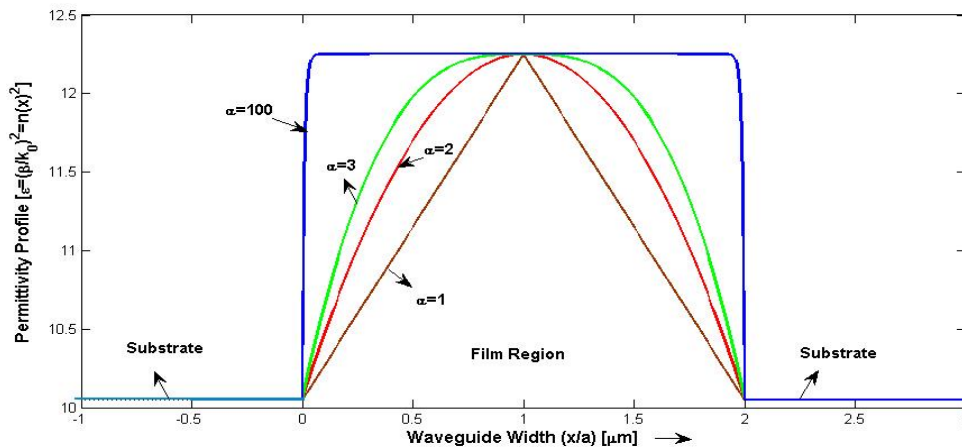


**Figure 2.** Schematic of $\alpha$-power refractive index profiles. Core width is $2\,\mu m$.

given by [27],

$$n^2\left(x\right) = \begin{cases} n_s^2 & (x < 0) \\ n_1^2 - \left(n_1^2 - n_s^2\right)\left|\frac{x}{a} - 1\right|^{\alpha}, & (0 \leq x \leq 2a) \\ n_s^2 & (x > 2a) \end{cases} \tag{1}$$

Next, we shows the results of FEM analyses for TE and TM modes in the $\alpha$-power refractive-index profiles given by Eq. (1). We assumed $n_1 = 3.5$, $n_s = 3.17$ and $a = 1\,\mu\text{m}$ throughout in all calculation.

Step index profile optical waveguide as shown in Figure 2 supports 4 TE and 4 TM guided modes as shown in Figure 3 at $\lambda = 1.55\,\mu\text{m}$. It is apparent from the plot that guided modes penetrate somewhat into the substrate region. Figure 3 reveals that various mode field profiles, only for fundamental $\text{TE}_{01}$
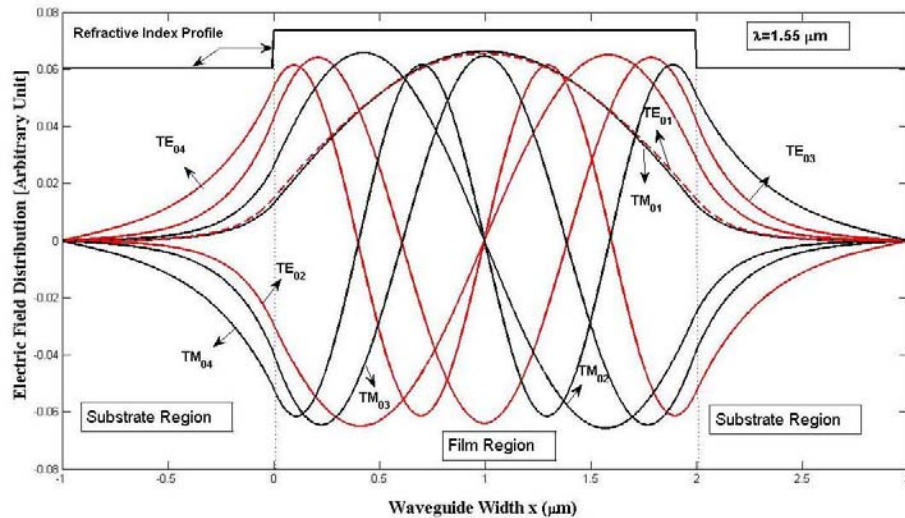


**Figure 3.** Step index profile optical waveguide structure supports 4 TE & 4 TM modes. Superimposed waveguide profile is scaled differently.
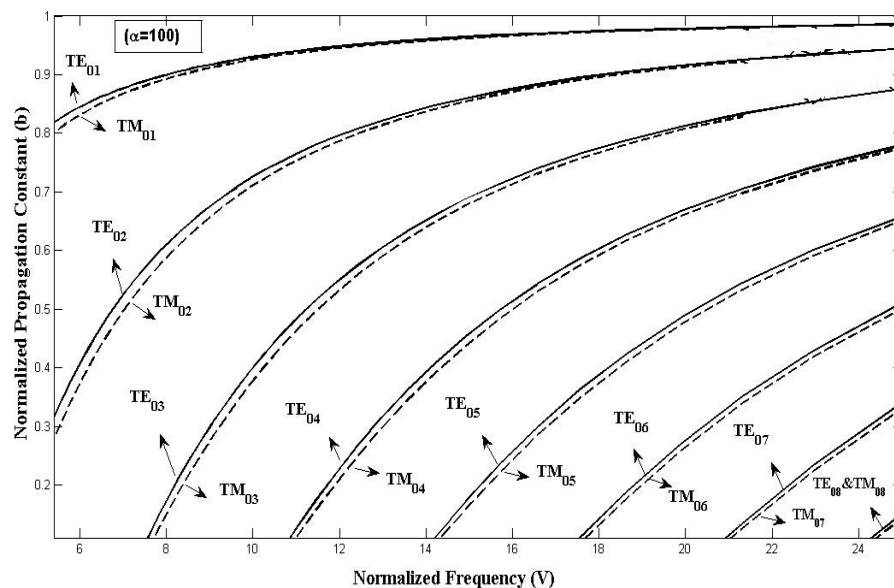


**Figure 4.** Universal graph in terms of normalized propagation constant (in terms of $b$) as a function of normalized frequency $V$-number for step index profile ($\alpha = 100$) case.

and $TM_{01}$ mode, are non-discriminable; however other higher order modes show $180°$ phase difference with each other.

Figure 4 shows the numerically simulated universal $b$-$V$ graph for step index profile case for the wide span of $V$-number. It is clear from Figure 4 that only lower order modes show some reasonable difference in propagation constant for only lower $V$-number region. However, as $V$-number increases higher order modes emerges while TE and TM modes become non-discriminable.

## 2.1. Triangular Refractive Index ($\alpha = 1$) Planar Slab Waveguide

Triangular index profile planar waveguide as shown in Figure 2 supports $3\,\mathrm{TE}$ and $3\,\mathrm{TM}$ guided modes as shown in Figure 5 at $\lambda = 1.55\,\mu\mathrm{m}$. It is apparent from Figure 5 that $TE_{02}$ and $TM_{02}$ modes are coincides. Incidentally, in contrast to step index profile, $TE_{01}$ and $TM_{01}$ modes are in opposite phases, hence they can be used as a mode filter.

Figure 6 shows the numerically simulated universal $b$-$V$ graph for triangular refractive index profile
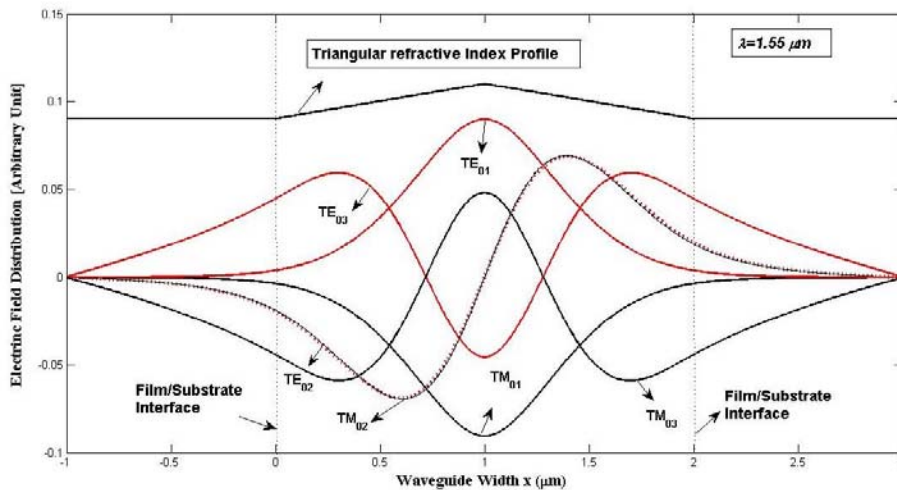


**Figure 5.** Triangular index profile optical waveguide structure supports $3\,\mathrm{TE}$ & $3\,\mathrm{TM}$ modes. Superimposed waveguide profile is scaled differently.
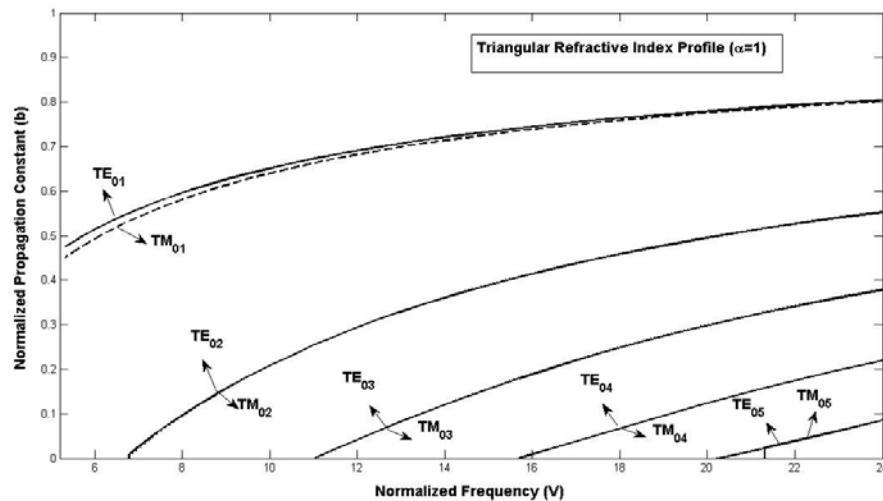


**Figure 6.** Universal graph in terms of normalized propagation constant (in terms of $b$) as a function of normalized frequency $V$-number for triangular index profile ($\alpha = 1$) case.

case for the wide span of $V$-number. It is clear from Figure 6 that only lower order modes show some reasonable difference in propagation constant for only lower $V$-number region. However, as $V$-number increases higher order modes emerge while TE and TM modes become non-discriminable.

## 2.2. Parabolic Refractive Index ($\alpha = 4$) Planar Slab Waveguide

Parabolic refractive index profile planar waveguide as shown in Figure 2 supports 4 TE and 4 TM guided modes as shown in Figure 7 at $\lambda = 1.55\,\mu\text{m}$. Interestingly it is apparent from Figure 7 that the entire TE/TM modes coincide in contrast to earlier cases. Hence they can be used as an all pass filter.

It is also clear from Figure 8 that only lower order modes show some reasonable difference in propagation constant for only lower $V$-number region. However, as $V$-number increases other higher order modes emerge while TE and TM modes become non-discriminable.
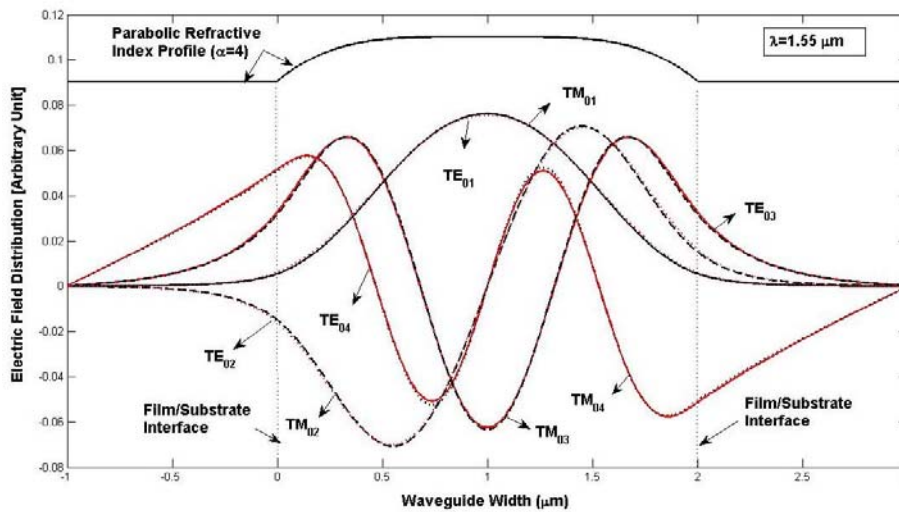


**Figure 7.** Parabolic refractive index profile optical waveguide structure supports 4 TE & 4 TM modes. Superimposed waveguide profile is scaled differently.
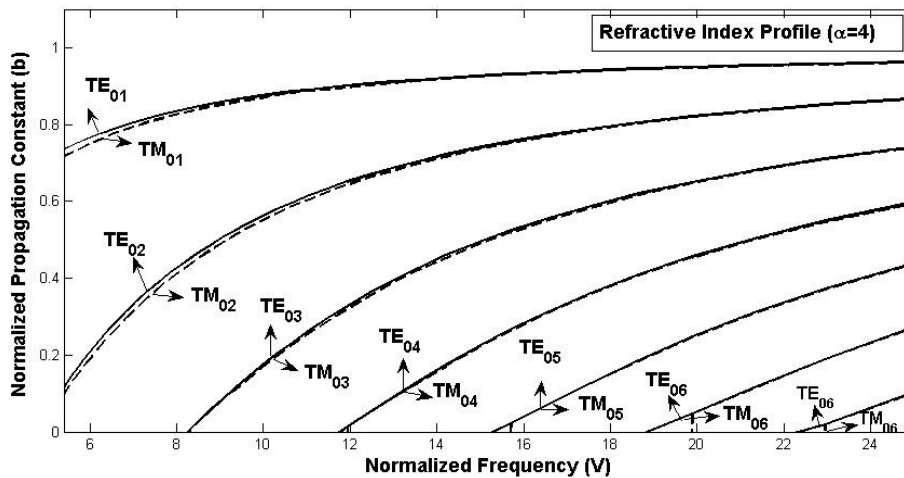


**Figure 8.** Universal graph in terms of normalized propagation constant (in terms of $b$) as a function of normalized frequency $V$-number for parabolic index profile ($\alpha = 4$) case.

## 3. MODE PROPAGATION, WAVEGUIDE DISPERSION AND CONFINEMENT FACTOR

Figures 4, 6 and 8 show the normalized propagation constant ($b$) versus $V$-number of arbitrary refractive index planar slab waveguide for various TE and TM modes. It is apparent that only the lowest order $TE_{01}$ or $TM_{01}$ modes support lower $V$-number of waveguide. Figure 9 shows the computed waveguide dispersion for the fundamental TE mode from the following expression [27]

$$D_W = -\frac{(n_1 - n_s)}{c\lambda} V \frac{d^2(V \cdot b)}{dV^2} \tag{2}$$

where $c$ is the velocity of light in vacuum. To compute the waveguide dispersion, we have used higher order polynomial technique as detailed in [27]. It is apparent that the waveguide dispersion is more
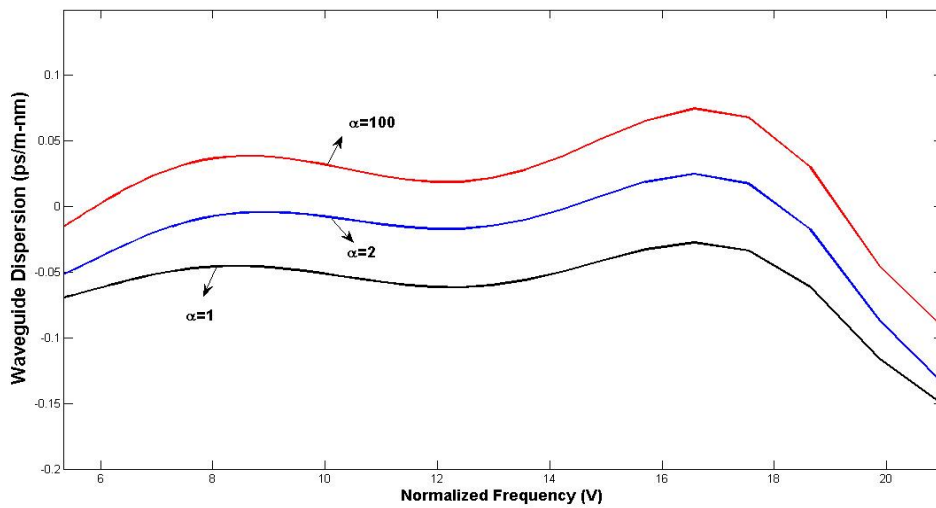


**Figure 9.** Waveguide dispersion ($D_W$) calculated for the lowest order $TE_{01}$ mode for the alpha power refractive index profile.
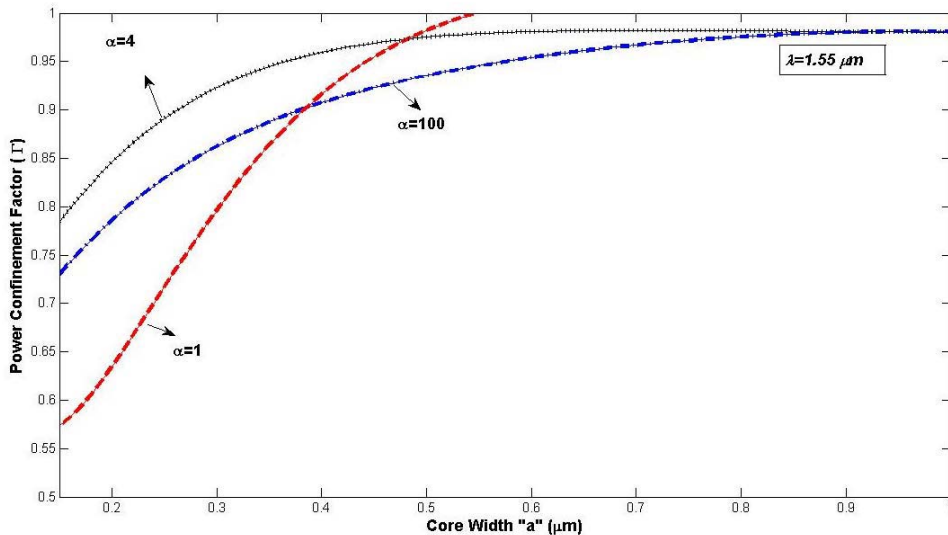


**Figure 10.** Power confinement factor ($\Gamma$) versus core width calculated for the lowest order $TE_{01}$ mode for the alpha power refractive index profile.

negative for triangular profile case comparatively to other cases in the entire wavelength range of interest. It is known through literature that higher order modes suffer less amount of waveguide dispersion than fundamental mode. Hence it is expected that higher modes having a triangular refractive index slab waveguide may suffer less amount of waveguide dispersion.

This may have a specific application for zero wavelength shifts while adding material dispersion to calculate the total dispersion in long haul systems. This also shows that by deploying the alpha power refractive index profile waveguide we can tune the zero dispersion wavelength from wide range of wavelength. Figure 10 shows the calculated power confinement factor ($\Gamma$) which is the ratio of power into the core versus total power in the computation window. It reveals that as the core width increased, substantial amount of power is confined into the core region, which is more prominent for the case of triangular refractive index profile case. It is also evident from the analysis that compared to step index profile, other profiles are more advantageous for longer wavelength application like while operating by DFB laser. If we compare Figures 3, 5 and 7, we can say that the fundamental mode shape which is more or less Gaussian has a sharp and high peak for the case of only triangular refractive index waveguide case.

Figure 11 shows the calculated power confinement factor versus wavelength for fundament mode case. It shows that confinement is low for the step index profile while it is high for the case of triangular ($\alpha = 1$) or parabolic profile ($\alpha = 2$) case. This effect is quite useful for high power delivery applications. It is known through literature that fundamental mode can carry maximum and confined power compared to other higher order modes.
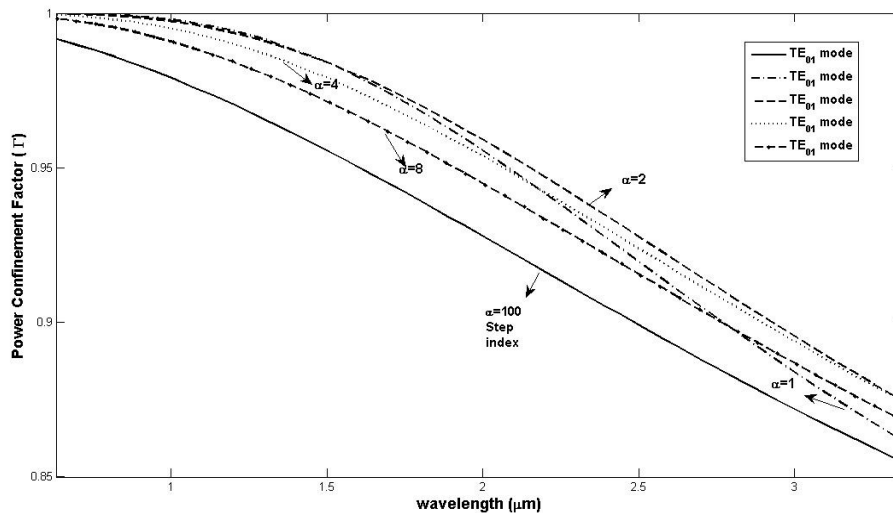


**Figure 11.** Power confinement factor ($\Gamma$) versus wavelength calculated for the lowest order mode for the alpha power refractive index profile.

## 4. BEAM PROPAGATION IN A $\alpha$-POWER REFRACTIVE INDEX PROFILE OF PLANAR SLAB WAVEGUIDES

We have computed allowed value of wave propagation constant $\beta$ for entire wavelength range by using finite element method [7, 27] and then launch the actual mode at $z = 0$ onto the $\alpha$-power waveguide structure. We have presented Gaussian field profile into modes with positive effective permittivity and into actual guided modes. It has been found while doing simulation that incident field can be well represented by some of the modes with positive effective refractive index.

Figure 12 shows a Gaussian beam which is a representation of positive effective index mode and cannot be distinguished with the actual Gaussian beam for the case of step index waveguide. However, the guided modes only deviate from the Gaussian shape of beam for this case. It has been found that incident field can be well represented by some of the modes with valid effective refractive index.
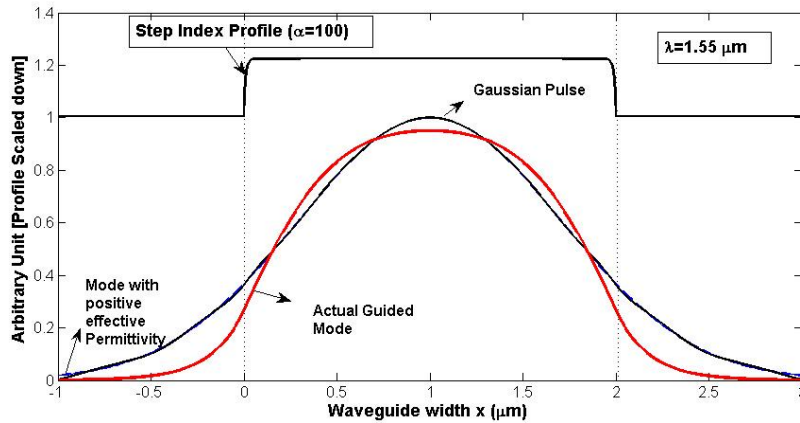
**Figure 12.** An actual guided mode which is deviated from Gaussian approximation of pulse represented at $x = 1\,\mu$m for the case of step index profile case.
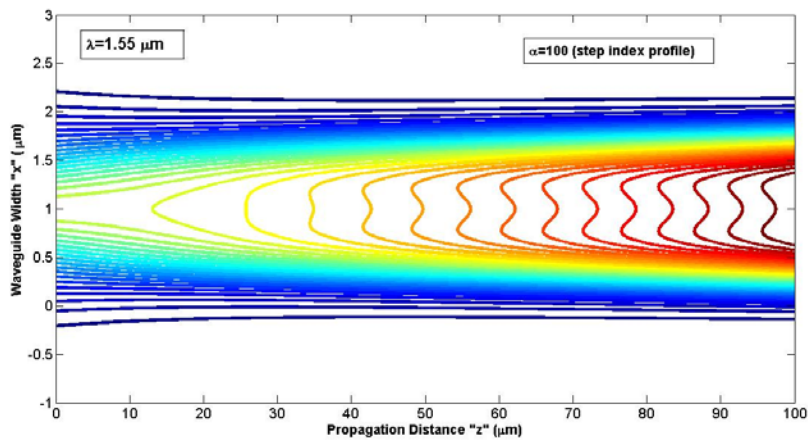


**Figure 13.** An incident beam having valid effective index as shown in Figure 12 propagates along a step index profile waveguide. We have plotted the contour plot for power $P(x; z)$ where $x$ runs from bottom to top and $z$, the propagation axis, from left to right.
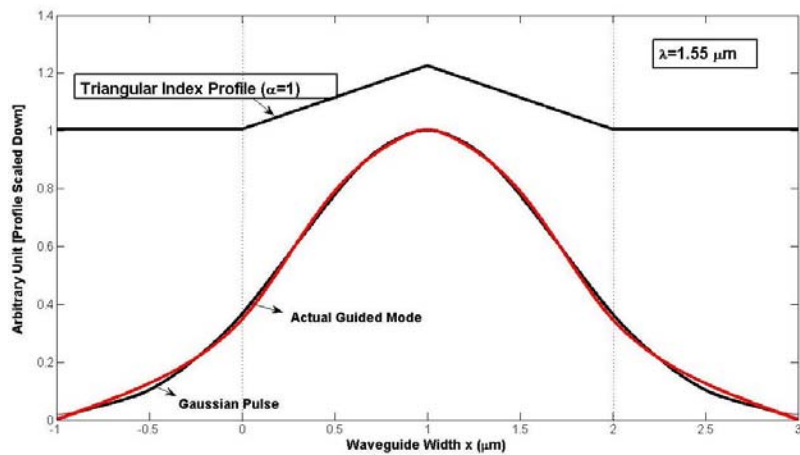


**Figure 14.** An actual guided mode which is very much resembled with Gaussian approximation of pulse represented at $x = 1\,\mu$m for the case of triangular index profile case.
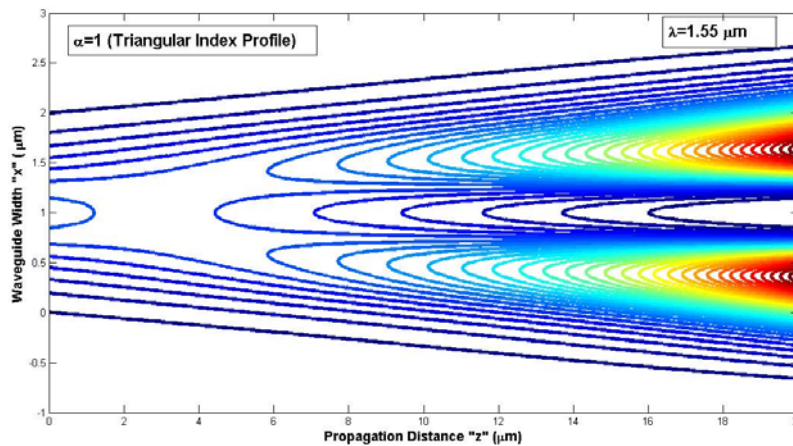
**Figure 15.** An incident beam having valid effective index as shown in Figure 14 propagates along a triangular index profile waveguide.
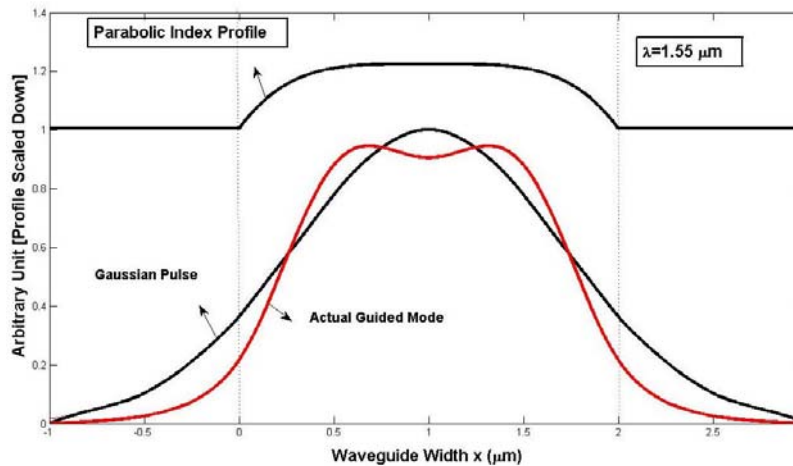


**Figure 16.** An actual guided mode which is deviated from Gaussian approximation of pulse represented at $x = 1\,\mu$m for the case of parabolic index ($\alpha = 4$) profile case.

In the present case, the overlap integral factor $R$ between the incidents Gaussian beam $f$ and its representation $g$ by guided modes which is defined by $|(g, f)|^2 = R(g, g)(f, f)$ turns out to be 0.9813. This is acceptable range as the Cauchy-Schwartz inequality says $0 \leq R \leq 1$. Figure 13 shows the field of Figure 12 with valid effective index launched at $x = 1\,\mu$m which then propagates along the $z$-direction with its appropriate propagation constant.

Figure 14 shows a Gaussian beam which is a representation of actual guided mode for the case of triangular refractive index waveguide. Figure 15 shows the field of Figure 14 with actual guided mode launched at $x = 1\,\mu$m which then propagates along the $z$-direction with its appropriate propagation constant. This is the special case when the guided mode is exactly resembled with the Gaussian pulse, hence it may have a very specific application in long haul communication systems. In the present case, the overlap integral factor $R$ between the incidents Gaussian beam $f$ and its representation $g$ by guided modes turns out to be 0.9912, which shows very good agreement for the actual guided mode. It is also apparent from Figure 15 that actual guided field is split into two equal parts after propagating over $z = 20\,\mu$m length over the waveguide. Figure 16 shows a Gaussian beam which is a representation of actual guided mode for the case of parabolic ($\alpha = 4$) refractive index waveguide. Figure 17 shows the field of Figure 16 with actual guided mode launched at $x = 1\,\mu$m which then propagates along the
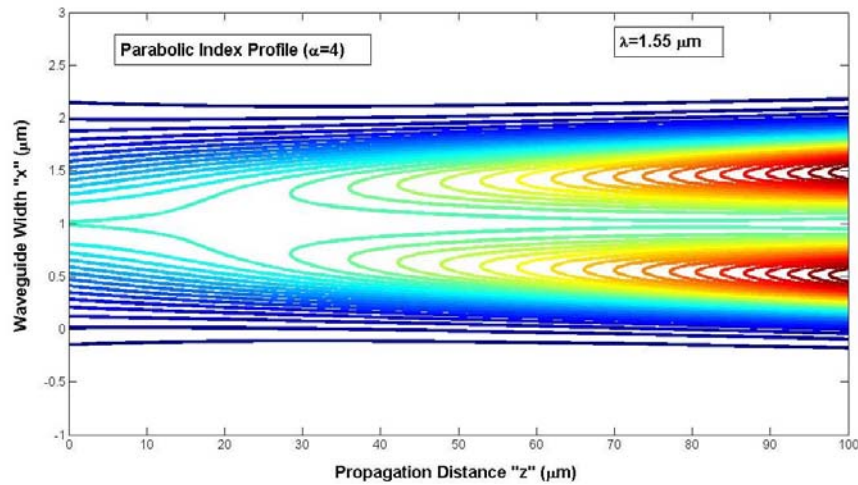
**Figure 17.** An incident beam having positive effective index as shown in Figure 16 propagates along a parabolic index profile waveguide.
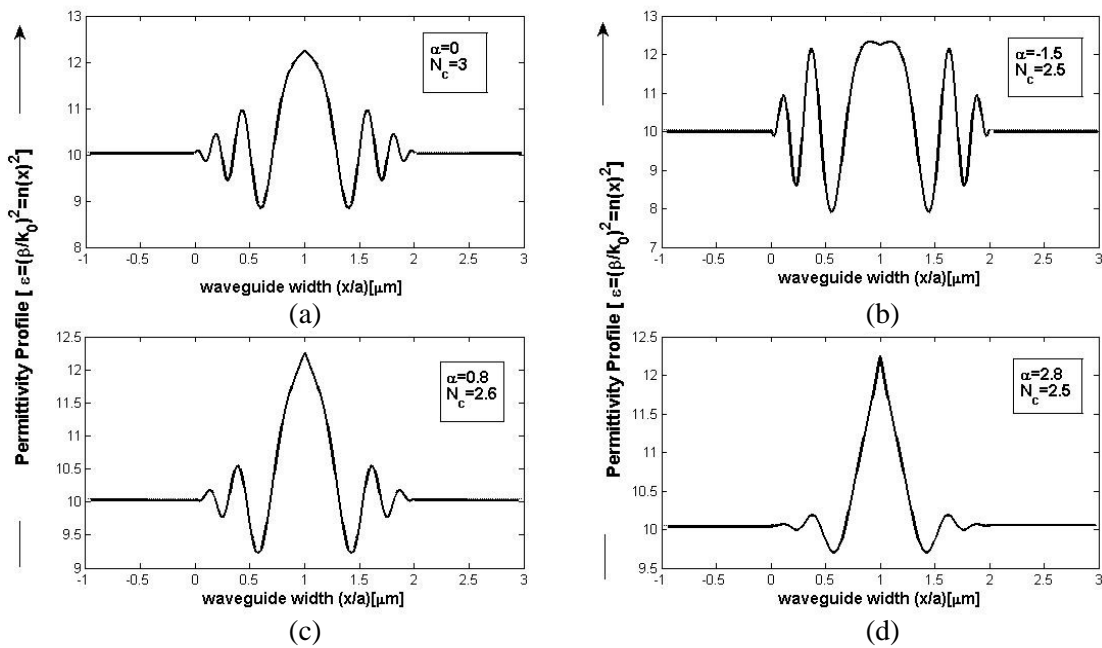


**Figure 18.** A variety of linearly chirp type refractive index profiles generated by varying refractive index profile parameters [31].

$z$-direction with its appropriate propagation constant. In this case the shape of guided mode is deviated with the Gaussian beam at centre portion.

In this case, the overlap integral factor $R$ between the incidents Gaussian beam $f$ and its representation $g$ by guided modes turns out to be 0.9747. This is also good resemblance with the actual guided mode. It is also apparent from Figure 17 that actual guided field is split into two equal part after propagation over $z = 100\,\mu$m length over the waveguide. This effect may be more prominent for this case due to an distortion in the initial launched pulse (guided mode) as evident from Figure 16. In the entire analysis of this section we have applied the mode propagation technique with transparent boundary condition [33].
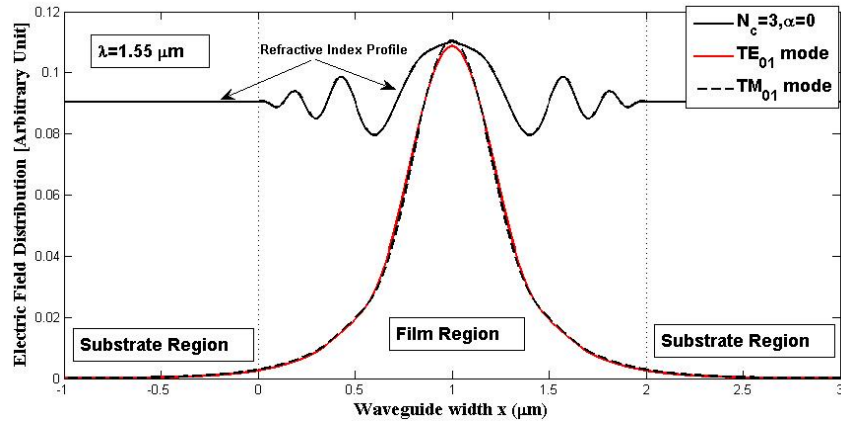
**Figure 19.** Chirped refractive profile ($N_c = 3$, $\alpha = 0$) waveguide structure support 1 TE & 1 TM modes. Superimposed waveguide profile is scaled differently.

## 5. CHARACTERIZATION OF LINEARLY CHIRP TYPES OF REFRACTIVE INDEX PROFILE OF PLANAR SLAB WAVEGUIDES

Now further we define a generalized linear chirp type refractive index profile which is a more complicated profile than the previous case and is defined as [27, 31],

$$n(x) = \begin{cases} n_1 - (n_1 - n_s)\left\{1 + \left|\dfrac{x}{a} - 1\right| - 1\right\}\exp\left(-\alpha\left|\dfrac{x}{a} - 1\right|\right)\cos\left\{2\pi N_c\left(\dfrac{x}{a} - 1\right)^2\right\} & 0 \le \dfrac{x}{a} \le 2 \\ n_1(1 - \Delta) & \left|\dfrac{x}{a}\right| > 2 \text{ and } 0 \end{cases} \tag{3}$$

where $n_1$ is the refractive index at the center of the waveguide at $x = a$; $\alpha$ controls the decay or growth of the profile envelope; $N_c$ is the number of cycles in a core radius; $a$ is the core radius; $n_s$ is the cladding or substrate refractive index. It can be noted that the parameters, which define the index profile can be divided in two parts. One is the fiber parameters such as $a$, $n_1$, $n_s$ and the profile parameters such as $\alpha$ and $N_c$. By varying these parameters ($a$, $n_s$, $n_1$, $N_c$, $\alpha$), one can generate profiles from simple step index type to complex multiple cladding type as shown in Figure 18. For an example, the profile parameters are $N_c = 0$ and $\alpha = 0$ respectively for step index profile. Now we show the results of our FEM analyses for TE and TM modes for the chirped types of refractive-index profiles given by Eq. (3). We assume $n_1 = 3.5$, $n_s = 3.17$ and $a = 1\,\mu\text{m}$ throughout in all cases. According to Figure 18, the core radius is $0 \le x \le 2a$. The chirped type of refractive profile corresponds to $N_c = 3$, $\alpha = 0$, as shown in Figure 18(a) and supports 1 TE and 1 TM guided modes as shown in Figure 19 at $\lambda = 1.55\,\mu\text{m}$. It is apparent from the plot that guided modes penetrate some-what into the substrate region. Figure 19 reveals that fundamental $TE_{01}$ and $TM_{01}$ modes are non-discriminable and resembled closely. This feature is quite contradictory to alpha power refractive index profile where many modes exist, and some of them are out of phase with each other. Figure 20 shows the numerically simulated universal $b$-$V$ graph for chirped profile ($N_c = 3$, $\alpha = 0$) case for the wide span of $V$-number. Apparently, only lower order mode shows significant difference in propagation constant for only lower $V$-number region. However, as $V$-number increases another mode emerges while TE and TM modes are still discriminable. This feature is unique compared to alpha power profile case, hence may have a specific application where TE and TM modes should be differentiable for all values of normalized frequency.

### 5.1. Chirped Refractive Index ($N_c = 2.5$, $\alpha = -1.5$) Profile Case

This case corresponds to Figure 18(b) and supports 1 TE and 1 TM guided modes as shown in Figure 21 at $\lambda = 1.55\,\mu\text{m}$. Interestingly, compared to Figure 19, the intensity of electric and magnetic fields differ more as the complexity of the refractive index increases. Figure 22 shows that the fundamental TE/TM
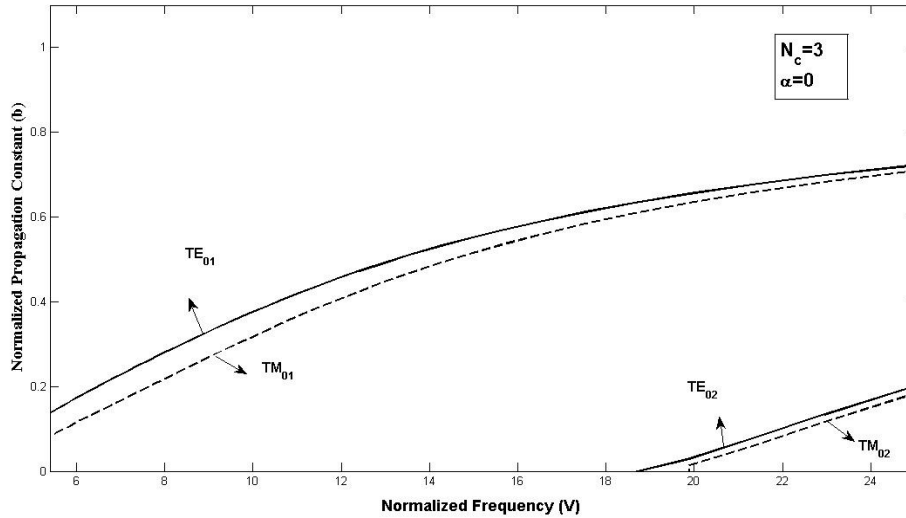
**Figure 20.** Computed universal graph in terms of normalized propagation constant $b$ as a function of normalized frequency $V$-number for chirped refractive profile ($N_c = 3$, $\alpha = 0$) case.
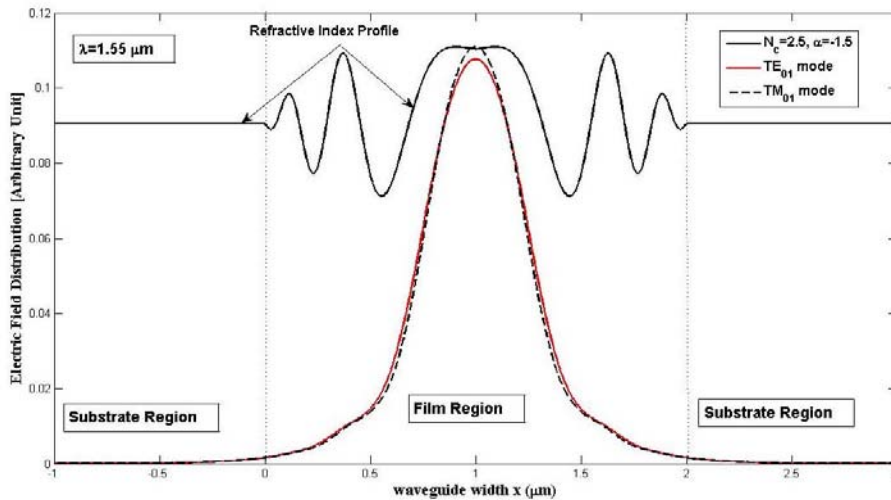


**Figure 21.** Chirped refractive profile ($N_c = 2.5$, $\alpha = -1.5$) waveguide structure support $1\,\mathrm{TE}$ & $1\,\mathrm{TM}$ modes. Superimposed waveguide profile is scaled differently.

mode differs substantially for lower $V$-number; however, difference is reduced for higher $V$-number case. The structure supports $4\,\mathrm{TE}$ and $4\,\mathrm{TM}$ modes for the entire range of normalized frequency. The large difference of field intensity and normalized propagation constant may have some specific applications in optical circulators or isolators.

## 5.2. Chirped Refractive Index ($N_c = 2.6$, $\alpha = 0.8$) Profile Case

This case corresponds to Figure 18(c) and supports $1\,\mathrm{TE}$ and $1\,\mathrm{TM}$ guided modes as shown in Figure 23 at $\lambda = 1.55\,\mu\mathrm{m}$. Interestingly, the intensity of electric and magnetic field patterns are opposite at the c-band wavelength on which the WDM optical system works due to low loss and compatible for optical amplifier. Figure 24 shows the computed universal $b$-$V$ graph for this case. The structure supports $2\,\mathrm{TE}/2\,\mathrm{TM}$ modes for the entire range of normalized frequency. The opposite field intensity pattern may have some specific applications in polarizer where we need to cut off the other field component.
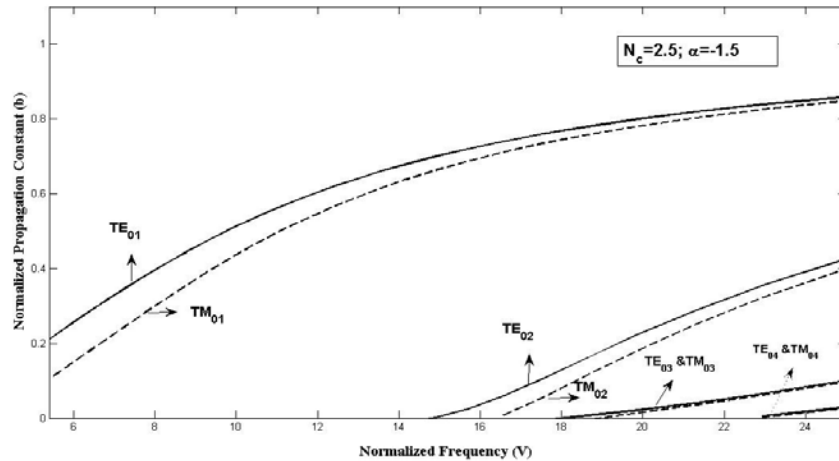
**Figure 22.** Calculated universal graph in terms of normalized propagation constant $b$ as a function of normalized frequency $V$-number for chirped refractive profile ($N_c = 2.5$, $\alpha = -1.5$) case.
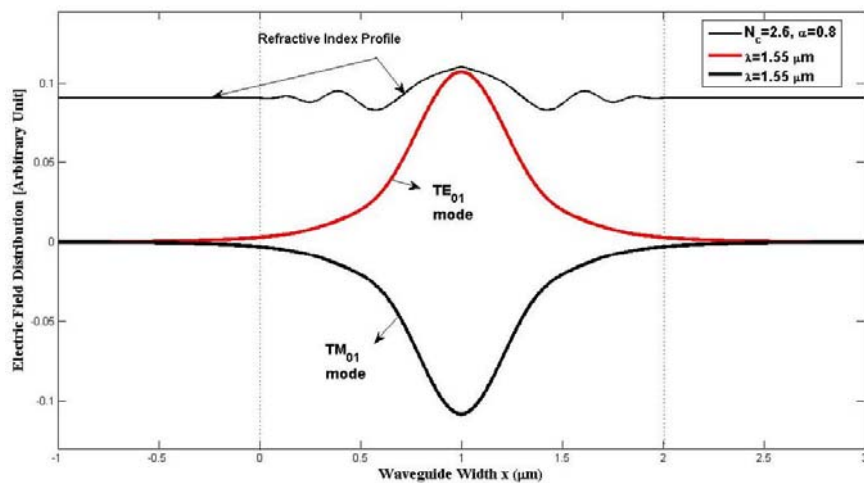


**Figure 23.** Chirped refractive profile ($N_c = 2.6$, $\alpha = 0.8$) waveguide structure support $1\,\mathrm{TE}$ & $1\,\mathrm{TM}$ modes with opposite field intensity pattern. Superimposed waveguide profile is scaled differently.

### 5.3. Chirped Refractive Index ($N_c = 2.5$, $\alpha = 2.8$) Profile Case

This case corresponds to Figure 18(d) and supports $1\,\mathrm{TE}/1\,\mathrm{TM}$ guided modes as shown in Figure 25 at $\lambda = 1.55\,\mu\mathrm{m}$. Indeed the electric and magnetic field intensities are in the same phase and intensity at c-band. Figure 26 shows the computed universal $b$-$V$ graph for this case. The structure supports $2\,\mathrm{TE}/2\,\mathrm{TM}$ modes for the entire range of normalized frequency. The normalized propagation constant $b$ differs for the entire operating frequency $V$, which is quite unusual compared to the previous case. The same field intensity pattern may have some specific applications in laser technology where we need to generate highly concentrated light beam.

### 6. WAVEGUIDE DISPERSION AND CONFINEMENT FACTOR FOR CHIRPED TYPE REFRACTIVE INDEX PROFILE WAVEGUIDE

Figures 20, 22, 24 and 26 show the normalized propagation constant ($b$) versus $V$-number of different chirped types of refractive index planar slab waveguide. Apparently, only the lowest order mode $\mathrm{TE}_{01}$
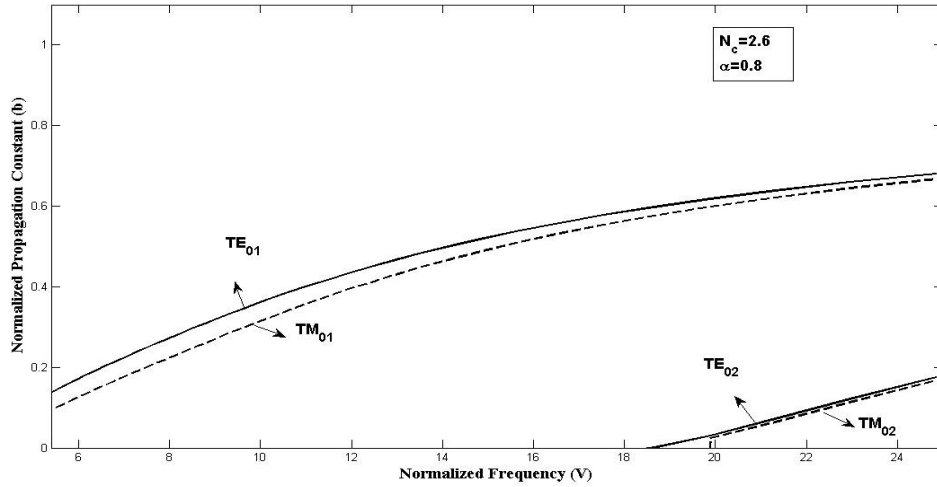
**Figure 24.** Calculated universal graph in terms of normalized propagation constant $b$ as a function of normalized frequency $V$-number for chirped refractive profile ($N_c = 2.6$, $\alpha = 0.8$) case.
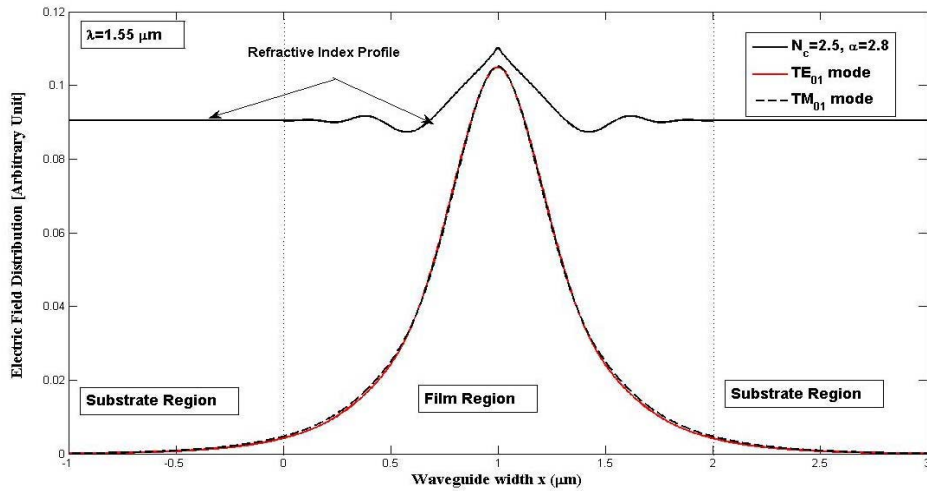


**Figure 25.** Chirped refractive profile ($N_c = 2.5$, $\alpha = 2.8$) waveguide structure supports 1 TE & 1 TM modes with exactly the same field intensity pattern. Superimposed waveguide profile is scaled differently.

or $TM_{01}$ supports lower $V$-number of waveguide. Figure 27 shows the computed waveguide dispersion for the fundamental TE mode from Eq. (2). As usual, to compute the waveguide dispersion, we use higher order polynomial technique [27]. Comparison shows that for the case of $N_c = 2.5$, $\alpha = -1.5$ waveguide dispersion is minimum for lower $V$-number but maximum for higher $V$-number; however the phenomena are reverse for the case of $N_c = 2.5$, $\alpha = 2.8$. It means that negative waveguide dispersion can be achieved by using more complicated profile such as dip in the centre of profile as shown in Figure 18(b). Figure 28 shows numerically calculated power confinement factor ($\Gamma$) versus wavelength for fundament mode case which is the ratio of power into the core versus total power in the computation window. It shows that confinement is low for the case of $N_c = 2.5$, $\alpha = 2.8$ while it is high for the case of $N_c = 2.5$, $\alpha = -1.5$ case. Again this result supports our finding that for the case of $N_c = 2.5$, $\alpha = -1.5$ the waveguide dispersion is minimum for lower $V$-number region. It can be said that the profile that corresponds to Figure 18(b) may be more useful for high power delivery applications in WDM optical systems.
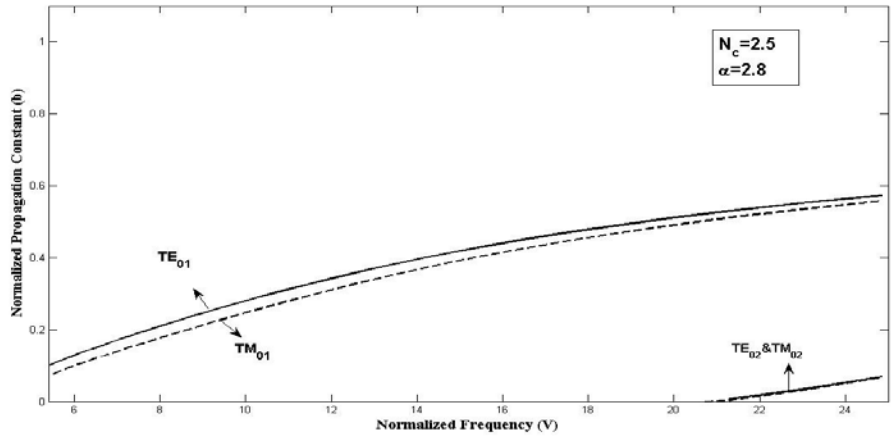
**Figure 26.** Calculated universal graph in terms of normalized propagation constant $b$ as a function of normalized frequency $V$-number for chirped refractive profile ($N_c = 2.5$, $\alpha = 2.8$) case.
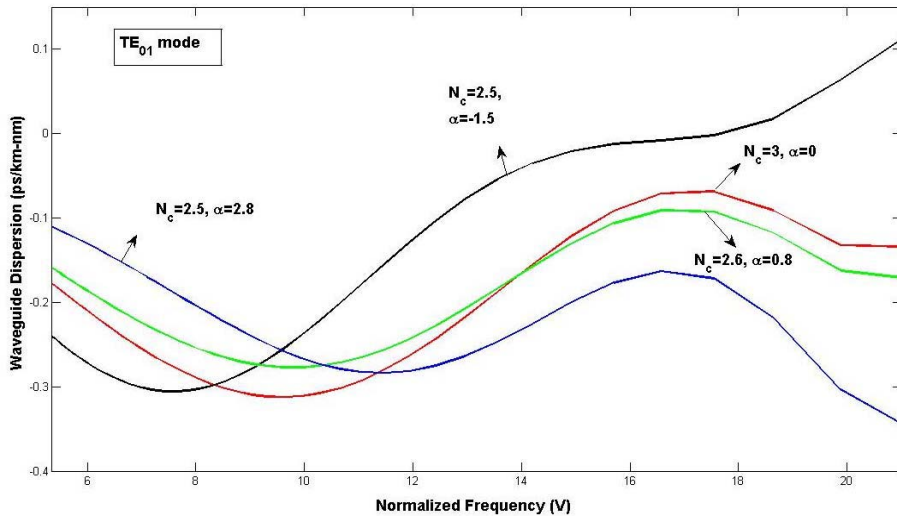


**Figure 27.** Waveguide dispersion ($D_W$) versus normalized frequency calculated for fundamental mode for the various chirp types of refractive index profile case.

## 7. MODE PROPAGATION IN A LINEARLY CHIRPED TYPES OF REFRACTIVE INDEX PROFILE OF PLANAR SLAB WAVEGUIDES

Prior to estimating the behavior of actual mode propagation through waveguide, we must know the allowed value of wave propagation constant $\beta$ for entire wavelength range [7, 27] and then ride the actual mode at $z = 0$ onto the chirped profile waveguide structure. Here too we have presented a Gaussian field profile into modes with valid effective permittivity as well as actual guided modes. It has been shown in earlier case that incident field can be well represented by some of the modes with valid effective refractive index, which is true for chirp profile too.

Figure 29 shows a Gaussian beam which is a representation of valid effective index mode and slightly distinguishable with the actual Gaussian beam for the case of chirp refractive index profile ($\alpha = 0$, $N_c = 3$) case. However, the guided modes quite deviate from the Gaussian shape of beam for this case. In the present case, the overlap integral factor $R$ between the incidents Gaussian beam $f$ and its representation $g$ by guided modes turns out to be 0.6860, which is an acceptable range as the
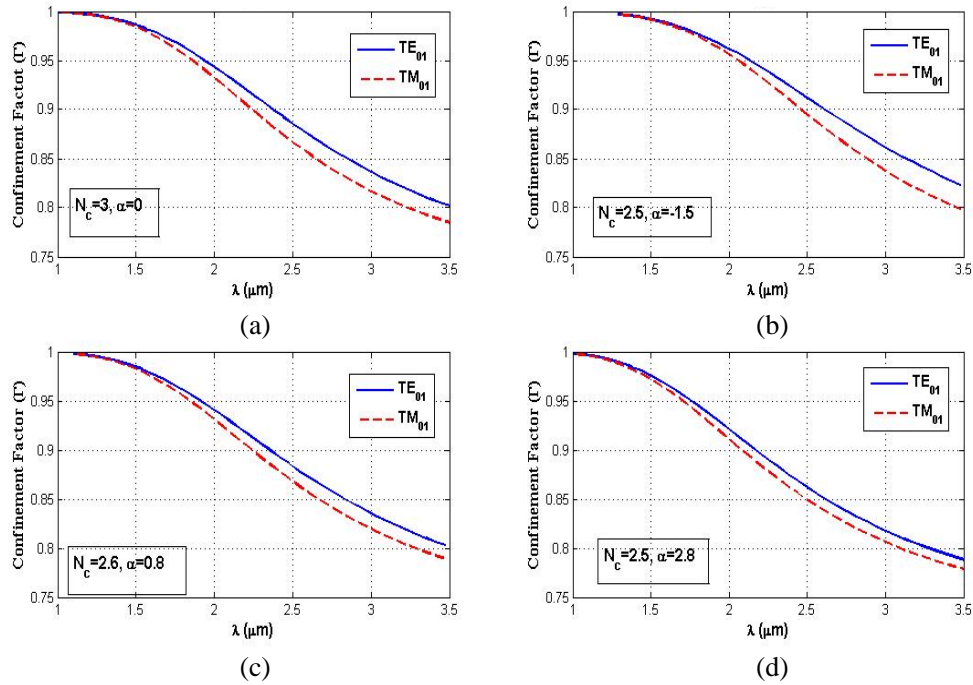
**Figure 28.** Power confinement factor ($\Gamma$) versus wavelength calculated for the lowest order mode for the various chirp types of refractive index profile case.
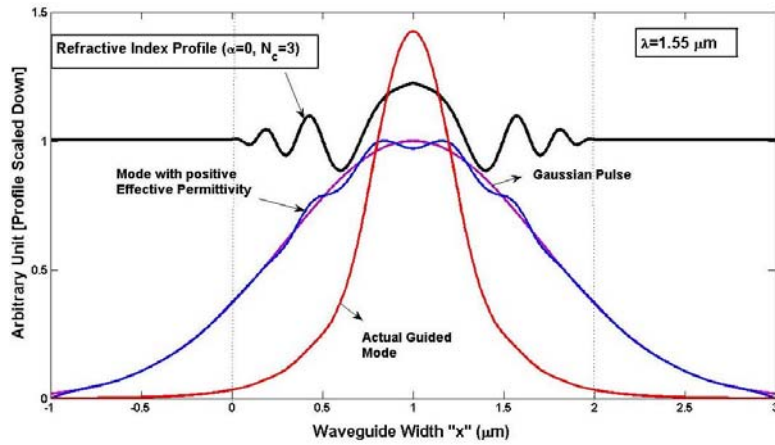


**Figure 29.** An actual guided mode which is deviated from Gaussian approximation of pulse represented at $x = 1\,\mu m$ for the case of chirp refractive index profile ($\alpha = 0$, $N_c = 3$) case.

Cauchy-Schwartz inequality says $0 \leq R \leq 1$. Hence our propagation result is valid. Figure 30 shows the field of Figure 29 with positive effective index launched at $x = 1\,\mu m$ which then propagates along the $z$-direction with its appropriate propagation constant.

Figure 31 shows a Gaussian beam which is a representation of actual guided mode for the case of chirp refractive index profile ($\alpha = -1.5$, $N_c = 2.5$) case. Figure 32 shows the field of Figure 31 with the actual guided mode launched at $x = 1\,\mu m$ which then propagates along the $z$-direction with its appropriate propagation constant. This is the special case when the guided mode is strongly deviated with the Gaussian pulse. As in the present case the overlap integral factor $R$ between the incidents Gaussian beam $f$ and its representation $g$ by guided modes turns out to be 0.6507. This is still under the acceptable range of validity. Figure 32 shows the actual guided mode propagation over $z = 100\,\mu m$
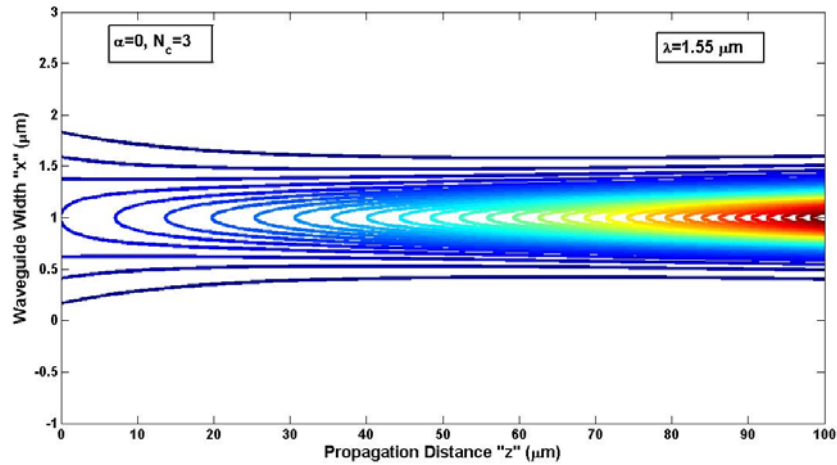
**Figure 30.** An incident beam having positive effective index as shown in Figure 29 propagates along a chirp refractive index profile ($\alpha = 0$, $N_c = 3$) case.
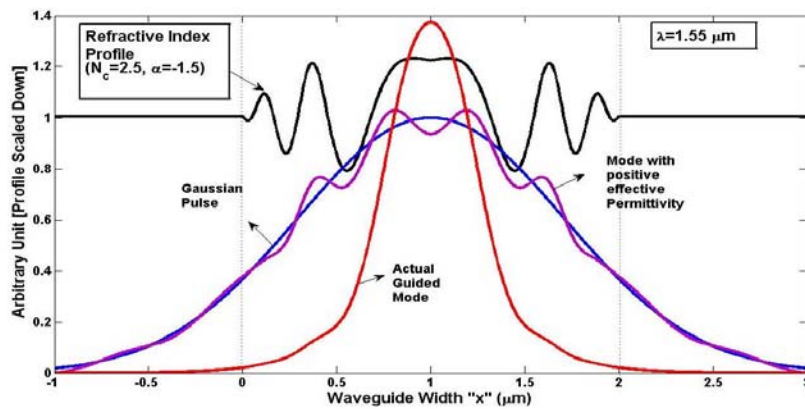


**Figure 31.** An actual guided mode which is deviated from Gaussian approximation of pulse represented at $x = 1\,\mu$m for the case of chirp refractive index profile ($\alpha = -1.5$, $N_c = 2.5$) case.
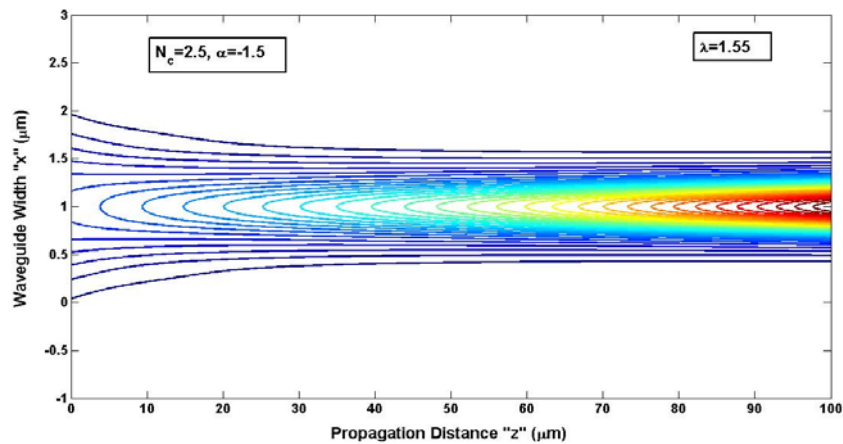


**Figure 32.** An incident beam having positive effective index as shown in Figure 31 propagates along a chirp refractive index profile ($\alpha = -1.5$, $N_c = 2.5$) case.
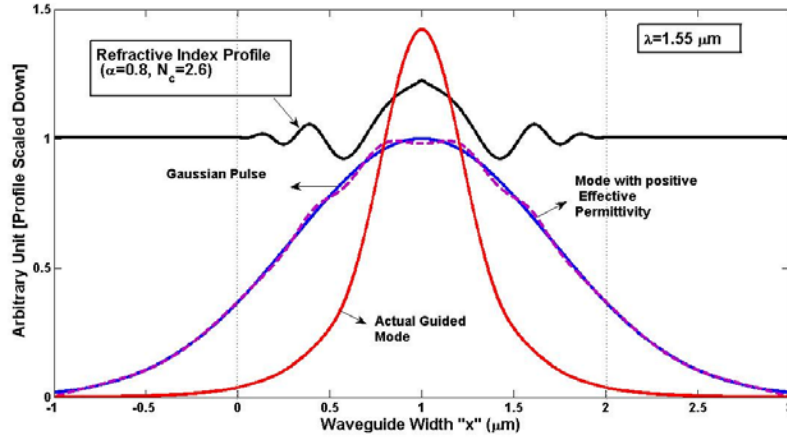
**Figure 33.** An actual guided mode which is deviated from Gaussian approximation of pulse represented at $x = 1\,\mu$m for the case of chirp refractive index profile ($\alpha = 0.8$, $N_c = 2.6$) case.
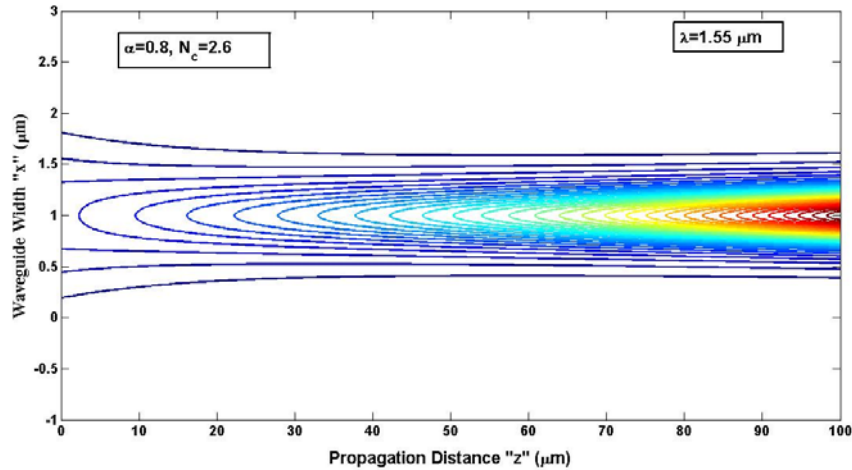


**Figure 34.** An incident beam having positive effective index as shown in Figure 33 propagates along a chirp refractive index profile ($\alpha = 0.8$, $N_c = 2.6$) case.
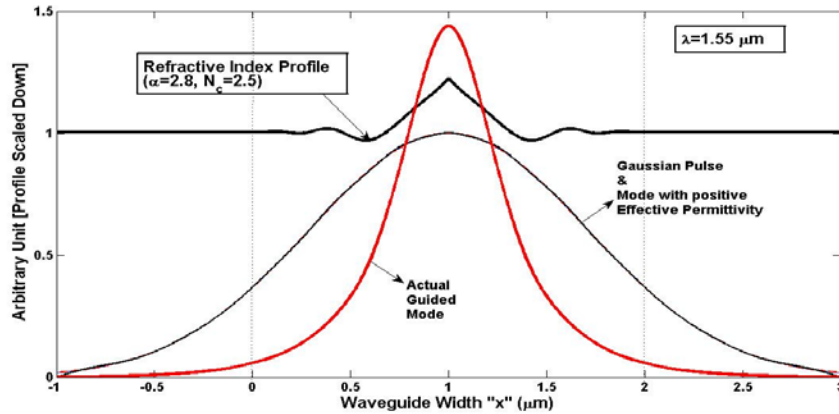


**Figure 35.** An actual guided mode which is deviated from Gaussian approximation of pulse represented at $x = 1\,\mu$m for the case of chirp refractive index profile ($\alpha = 2.8$, $N_c = 2.5$) case.
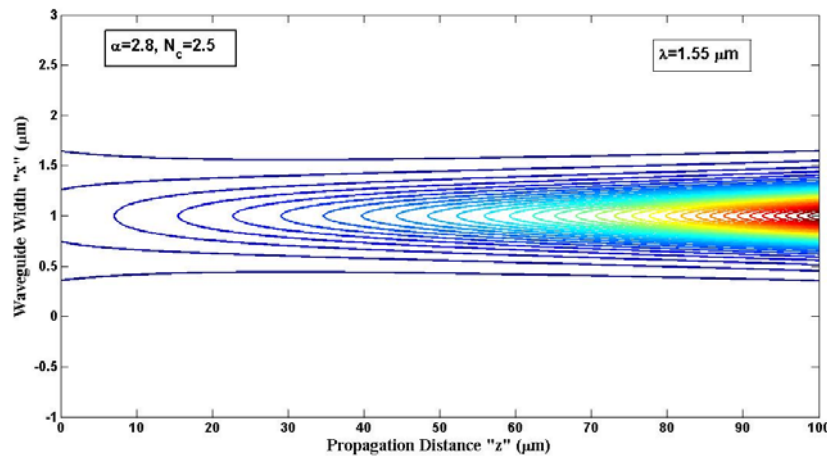
**Figure 36.** An incident beam having positive effective index as shown in Figure 35 propagates along a chirp refractive index profile ($\alpha = 2.8$, $N_c = 2.5$) case.

length of waveguide. It shows that the pulse shape remains preserved except the broadening as contrary to alpha power refractive index profile case. Hence the chirp profile will be more useful than alpha power refractive index profile. Figure 33 shows a Gaussian beam which is a representation of actual guided mode for the case of chirp refractive index profile ($\alpha = 0.8$, $N_c = 2.6$) case. In this case, the overlap integral factor between the incidents Gaussian beam and its representation by guided modes turns out to be 0.7042. Figure 34 shows the field of Figure 33 with actual guided mode launched at $x = 1\,\mu$m which then propagates along the $z$-direction with its appropriate propagation constant. In this case, the shape of guided mode remains more or less preserved too except broadening.

Figure 35 shows a Gaussian beam which is a representation of actual guided mode for the case of chirp refractive index profile ($\alpha = 2.8$, $N_c = 2.5$). In this case, the overlap integral factor between the incidents Gaussian beam and its representation by guided modes turns out to be 0.7515. Figure 36 shows the field of Figure 35 with actual guided mode launched at $x = 1\,\mu$m which then propagates along the $z$-direction with its appropriate propagation constant. In the entire analysis of this section, as compared to previous analysis, we have applied the mode propagation technique with transparent boundary condition [33].

## 8. CONCLUSION

In the conclusion of the paper, we have characterized the properties of graded/linearly chirp types of refractive index profile. We have demonstrated how the actual mode in the form of input beam propagates through $\alpha$-power refractive index profile waveguide. We then characterize the waveguide in terms of $\alpha$-power and chirped types of refractive index profile while considering both the TE and TM mode cases. Initially we have used the Finite Element Method to compute the allowed value of propagation constant then applied the Beam propagation method with transparent condition to demonstrate the pulse propagation in the form of actual mode. Then waveguide dispersion, guided mode profile, power confinement factor and universal $b$-$V$ graph are estimated for various cases. It has been demonstrated that for the step index profile case all the TE/TM modes differ substantially compared to triangular and parabolic index profile case. It is also observed that except for step index profile case higher order TE/TM modes are almost smeared for $\alpha = 1$, $\alpha = 4$ profile cases. The main aim of this paper is to establish a strong comparison between alpha power refractive index profiles and chirped refractive index profile waveguide to analyze the TE/TM mode numerically followed by characterization. Then we apply the mode propagation concept to estimate the propagation phenomena in alpha and chirp type refractive index profile waveguide. We have substantiated the importance of triangular/chirped types of refractive index planar slab waveguide while comparing with other cases. It is because of its high power confinement factor, low waveguide dispersion properties; fundamental

mode shape is an exactly Gaussian shape. Hence triangular index profile followed by chirped types of refractive index profile waveguide seems to be more useful for high power delivery and long haul optical communication systems. In fact, chirped type refractive index profile waveguide shows no pulse distortion except broadening compared to alpha power refractive index profile waveguide hence will be more useful in optical communication systems where low dispersion link has to be deployed.

## ACKNOWLEDGMENT

## REFERENCES

1. Zheludev, N. I., "Photonic-plasmonic devices: A 7-nm light pen makes its mark," *Nat. Nanotechnol.*, Vol. 5, 10–11, 2010.
2. Politano, A. and G. Chiarello, "Quenching of plasmons modes in air-exposed grapheme-Ru contacts for plasmonic devices," *Appl. Phy. Lett.*, Vol. 102, 201608, 2013.
3. He, X. Y., Q. J. Wang, and S. F. Yu, "Numerical study of gain-assisted terahertz hybrid plasmonic waveguide," *Plasmonics*, Vol. 7, 571–577, 2012.
4. Baqir, M. A. and P. K. Choudhary, "Dispersion characteristics of optical fibers under PEMC twist," *Journal of Electromagnetic Wave and Application*, Vol. 28, No. 17, 2124–2134, 2014.
5. Li, Z., K. Bao, Y. Fang, Y. Huang, P. Nordlander, and H. Xu, "Correlation between incident and emission polarization in nanowire surface plasmons waveguide," *Nano. Lett.*, Vol. 10, 1831–1835, 2010.
6. Politano, A. and G. Chiarello, "Unravelling suitable grapheme-metal contacts for grapheme-based plasmonic device," *Nanoscale*, Vol. 5, 8251–8220, 2013.
7. Raghuwanshi, S. K. and S. Kumar, "Waveguide dispersion characteristics of graded/linearly chirp type's refractive index profile of planar slab optical waveguide by using the modified finite element method," *Journal of Optics*, Springer, Aug. 12, 2014, Doi: 10.1007/s12596-014-0220-y.
8. Mussina, R., D. R. Selviah, F. A. Fernnandez, A. G. Tijhuis, and B. P. D. Hon, "A rapid accurate technique to calculate the group delay dispersion and dispersion slop of arbitrary radial refractive index profile weakly-guiding optical fibers," *Progress In Electromagnetics Research*, Vol. 145, 99–113, 2014.
9. Walpita, L. M., "Solution for planar optical waveguide equation by selecting zero elements in a characteristics matrix," *Journal of the Optical Society of America*, Vol. A2, 592–602, 1985.
10. Rahman, B. M. A., "Finite element analysis of optical waveguides," *Progress In Electromagnetics Research*, Vol. 10, 187–216, 1995.
11. Honkis, T. H., "Analysis of optical waveguide with arbitrary index profile using an immersed interface method," *International Journal of Modern Physics C*, Vol. 22, No. 7, 687–710, 2011.
12. Okoshi, T. and K. Okamoto, "Analysis of wave propagation in inhomogeneous optical fibers using a varational method," *IEEE Trans. on Microwave Theory and Tech.*, Vol. 22, No. 11, 938–945, 1974.
13. Popescu, V. A., "Determination of normalized propagation constant for optical waveguide by using second order variational method," *Journal of Optoelectronics and Advanced Mat.*, Vol. 7, No. 5, 2783–2786, 2005.
14. Rostami, A. and H. Motavali, "Asymptotic iteration method: A power approach for analysis of inhomogeneous dielectric slab waveguide," *Progress In Electromagnetics Research B*, Vol. 4, 171–182, 2008.

15. Chaudhuri, P. R. and S. Roy, "Analysis of arbitrary index profile planar optical waveguide and multilayer nonlinear structure: A simple finite differences algorithm," *Opt. Quant. Electron.*, Vol. 39, 221–237, 2007.

16. Sadiku, M. N. O., *Numerical Techniques in Electromagnetic,* 2nd Edition, CRC Press LLC, 1992.

17. Booton, R. C., *Computational Methods for Electromagnetic and Microwave,* John Wiley and Sons, 1992.

18. Kasim, N. M., A. B. Mohammad, and M. H. Ibrahim, "Optical waveguide modeling based on scalar finite difference scheme," *Journal Teknologi.*, Vol. 45(D), 181–194, 2006.

19. Gambling, W. A., D. N. Payne, and H. Matsumura, "Cut-off frequency in radically inhomogeneous single mode fiber," *Electron. Letters*, Vol. 13, No. 5, 130–140, 1977.

20. Zhuangqi, C., Y. Jiang, and C. Yingli, "Analytical investigation of planar optical waveguide with arbitrary index profiles," *Optical and Quant. Electronics*, Vol. 31, 637–644, 1999.

21. Chiang, K. S., "Review of numerical and approximation methods for modal analysis of general dielectric waveguide," *Opt. Quant. Electron.*, Vol. 26, 113–134, 1994.

22. Xu, W., Z. H. Wang, and Z. M. Huang, "Propagation constant of a planar dielectric waveguide with arbitrary refractive index variation," *Opt. Lett.*, Vol. 18, 805–807, 1993.

23. Okamoto, K., *Fundamentals of Optical Waveguide,* Academic Press, 2006.

24. Sharma, E. K., I. C. Goyal, and A. K. Ghatak, "Calculation of cut-off frequencies in optical fibers for arbitrary profiles using the matrix method," *IEEE Journal of Quant. Electron.*, Vol. 17, No. 12, 2317–2320, 1981.

25. Okamoto, K. and T. Okoshi, "Analysis of wave propagation in optical fibers having core with $\alpha$-power refractive distribution and uniform cladding," *IEEE Trans. on Microwave Theory and Tech.*, Vol. 24, No. 7, 416–421, 1976.

26. Raghuwanshi, S. K. and S. Kumar, "Analytical expression for dispersion properties of circular core dielectric waveguide without computing $d^2\beta/dk^2$ numerically," *I-manager's Journal on Future Engineering & Technology*, Vol. 7, No. 3, 26–34, 2012.

27. Raghuwanshi, S. K., S. Kumar, and A. Kumar, "Dispersion characteristics of complex refractive-index planar slab optical waveguide by using finite element method," *Optik*, Vol. 125, No. 20, 5929–5935, Elsevier, Oct. 2014.

28. Ghatak, A. K. and K. Thyagarajan, *Optical Electronics: Introduction to Fiber Optics,* Cambridge Press, 1999.

29. Hotate, K. A. and T. Okoshi, "Formula giving single-mode limit of optical fiber having arbitrary refractive index profile," *Electron. Letters*, Vol. 14, No. 8, 246–248, 1978.

30. Rostami, A. and S. K. Moyaedi, "Exact solution for the TM mode in inhomogeneous slab waveguides," *Laser Physics*, Vol. 14, No. 12, 1492–1498, 2004.

31. Survaiya, S. P. and R. K. Shevagaonkar, "Dispersion characteristics of an optical fiber having linear chirp refractive index profile," *IEEE Journal of Lightwave Tech.*, Vol. 17, No. 10, 1797–1805, 1999.

32. Raghuwanshi, S. K. and S. Talabattula, "Dispersion and peak reflectivity analysis in a non-uniform FBG based sensors due to arbitrary refractive index profile," *Progress In Electromagnetics Research B*, Vol. 36, 249–265, 2012.

33. Hadley, G. R., "Transparent boundary condition for beam propagation," *Opt. Lett.*, Vol. 16, 624–626, 1991.